

University of Nebraska - Lincoln

DigitalCommons@University of Nebraska - Lincoln

---

Biomedical Imaging and Biosignal Analysis  
Laboratory

Biological Systems Engineering

---

5-1996

# Ultrasound Three- Dimensional Velocity Measurements by Feature Tracking


Gregory R. Bashford

*University of Nebraska - Lincoln*, [gbashford2@unl.edu](mailto:gbashford2@unl.edu)

Olaf T. von Ramm

*Duke University*, [grb@acpub.duke.edu](mailto:grb@acpub.duke.edu)

Follow this and additional works at: <http://digitalcommons.unl.edu/biba>

 Part of the [Biochemistry, Biophysics, and Structural Biology Commons](#), [Bioinformatics Commons](#), [Health Information Technology Commons](#), [Other Analytical, Diagnostic and Therapeutic Techniques and Equipment Commons](#), and the [Systems and Integrative Physiology Commons](#)

---

Bashford, Gregory R. and von Ramm, Olaf T., "Ultrasound Three- Dimensional Velocity Measurements by Feature Tracking" (1996). *Biomedical Imaging and Biosignal Analysis Laboratory*. 1. <http://digitalcommons.unl.edu/biba/1>

This Article is brought to you for free and open access by the Biological Systems Engineering at DigitalCommons@University of Nebraska - Lincoln. It has been accepted for inclusion in Biomedical Imaging and Biosignal Analysis Laboratory by an authorized administrator of DigitalCommons@University of Nebraska - Lincoln.

# Ultrasound Three-Dimensional Velocity Measurements by Feature Tracking

Gregory R. Bashford, *Student Member, IEEE*, and Olaf T. von Ramm

**Abstract**— This article describes a new angle-independent method suitable for three-dimensional (3-D) blood flow velocity measurement that tracks features of the ultrasonic speckle produced by a pulse echo system. In this method, a feature is identified and followed over time to detect motion. Other blood flow velocity measurement methods typically estimate velocity using one- (1-D) or two-dimensional (2-D) spatial and time information. Speckle decorrelation due to motion in the elevation dimension may hinder this estimate of the true 3-D blood flow velocity vector. Feature tracking is a 3-D method with the ability to measure the true blood velocity vector rather than a projection onto a line or plane. Off-line experiments using a tissue phantom and a real-time volumetric ultrasound imaging system have shown that the local maximum detected value of the speckle signal may be identified and tracked for measuring velocities typical of human blood flow. The limitations of feature tracking, including the uncertainty of the peak location and the duration of the local maxima are discussed. An analysis of the expected error using this method is given.

## I. INTRODUCTION

**I**N A scattering environment in which many subresolution scatterers occupy a resolution cell, such as in the human body, ultrasound echo signals add both constructively and destructively to produce a phenomenon called speckle [1]. In a B-mode image, speckle appears as a mottled pattern on top of anatomic structures. Speckle reduces the visual image quality of the data [2] and limits the ability to discern fine structure in the picture; thus, speckle may obstruct the view of clinically useful information.

However, speckle is useful in the determination of target motion. Doppler processors code differences in arrival times from speckle signals to instantaneous phase information of a master clock to calculate a one-dimensional (1-D) projection of the velocity of the moving tissue [3]. Doppler, a 1-D process, suffers from aliasing and angle dependence. Aliasing is usually not a problem in clinical diagnosis, since clinicians have learned to use this effect as a marker for turbulence and high-speed jets. In addition, commercial instruments permit shifting of the baseline which can extend the velocity limits displayed. However, flow parallel to the face of the transducer will be hidden due to angle dependence. To date, no commercial machine gives directional flow information in more than one dimension.

Manuscript received August 21, 1995; revised December 18, 1995. This work was supported in part by Health and Human Services Grant NCI CA37586 and National Science Foundation/Engineering Research Center Grant CDR-8622201.

The authors are with the Department of Biomedical Engineering, Duke University, Durham, NC 27708 USA (e-mail: grb@acpub.duke.edu).

Publisher Item Identifier S 0885-3010(96)03100-0.

Two-dimensional (2-D) flow algorithms have been researched for several years. Multiple transducers can provide flow information in more than one dimension if the transducers are mounted favorably; in this approach, each transducer provides one projection of the velocity vector [4], [5]. In another example, Phillips is presently constructing a 2-D color flow system that electronically divides one phased-array transducer into two independently steered subtransducers [6]. Each subtransducer resolves one component of the true velocity flow vector in real time using pulsed-wave (PW) Doppler.

Correlation methods use a statistical comparison of the speckle pattern from one interrogation to the next [7]. Abandoning the Doppler-based algorithms, Trahey has developed and constructed a real-time 2-D color flow system built at Duke University that utilizes a 2-D cross-correlation technique [8]. Also, Ferrara has introduced a flow estimation method which determines velocity by estimating the lateral transit time across the ultrasound beam [9]. Newhouse has estimated velocity by using information derived from the bandwidth of the received signal [10]. Meunier *et al.* used the spatial gradient at a point in an image to determine velocity maps incorporating translation, rotation, and deformation of the speckle pattern for heart motion analysis [18].

In 1991, Roundhill first proposed extracting a peak of the amplitude of the detected speckle signal and tracking it in successive interrogations for measuring axial flow [11]. This peak was labeled as a directly measured *feature*. His real-time system performed this technique accurately in one dimension. The advantage of feature tracking is that it selectively extracts easily identifiable parts of the speckle signal, reducing the amount of information being processed, which makes it computationally simpler than other flow algorithms.

We hypothesized that Roundhill's method could be extended to three dimensions, and that speckle actually has a peak locatable in three dimensions. We further hypothesized that this peak could be identified, and that it would move in correspondence with the local blood or tissue motion. In a previous paper [12], we characterized the three-dimensional (3-D) nature of speckle by identifying and describing 3-D features corresponding to the peak brightness level (local maxima) of speckle. These peaks have a distinct distribution (in amplitude) in a volume. Also, the peaks have a  $-6$ -dB breadth, about twice that predicted by the full width at half maximum (FWHM) along the lateral axis of the 3-D autocovariance function (ACVF). An example of a visualization of two of these features is shown in Fig. 1. This figure is a contour

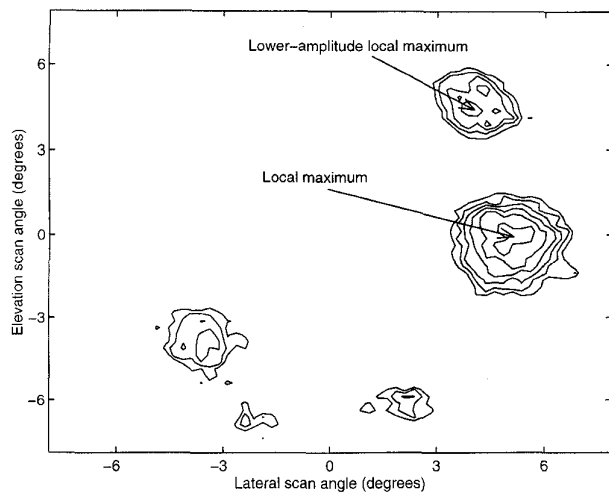


Fig. 1. Contour map in the elevation-lateral plane of local maxima. The contours represent  $-1$  dB levels down from the global maximum in the plane.

map in the elevation-lateral plane, or plane parallel to the transducer face (i.e., a C-scan), showing two local maxima in a volume of speckle data. The contours represent  $-1$  dB levels down from the global maximum in the plane. The figure represents a small area which measures only  $15^\circ$  across laterally at a depth of about  $70$  mm, i.e., the field of view is about  $18$  mm on each side. In addition, only the amplitudes within  $6$  dB from the global maximum are displayed; thus more local maxima may be present than are shown.

Our process detects blood flow by the identification and tracking of speckle features in an acoustic field. The 3-D local maximum is chosen as a feature to track; alternatively, the 3-D minima or "valleys" might be chosen. However, since the valley is a low-amplitude value, detecting it may be more difficult since it is prone to be hidden under the noise floor. By utilizing a volume of data, the position of the chosen feature is measured and tracked in three dimensions. The added spatial information of tissue motion, i.e., the magnitude and direction of the movement in the elevation dimension, may be clinically useful in cardiovascular diagnosis. If the tissue in consideration is blood, the information is in regard to the 3-D velocity vector of blood flow.

In order to test the hypothesis that speckle peaks can be used to determine and quantify tissue motion, experiments were performed in which a transducer, acquiring 3-D scan data, was translated over a scattering phantom to simulate tissue motion. Individual peaks were selected and tracked to see if their movement corresponded with the applied translation. Errors encountered in estimating motion were analyzed, and a model predicting the magnitude of error to be expected was derived.

## II. MATERIALS AND METHODS

### A. Experimental Materials

The experimental setup used in the feature-tracking experiments is shown in Fig. 2. The Duke University phased array system [13], a real-time 3-D ultrasound imaging system, was

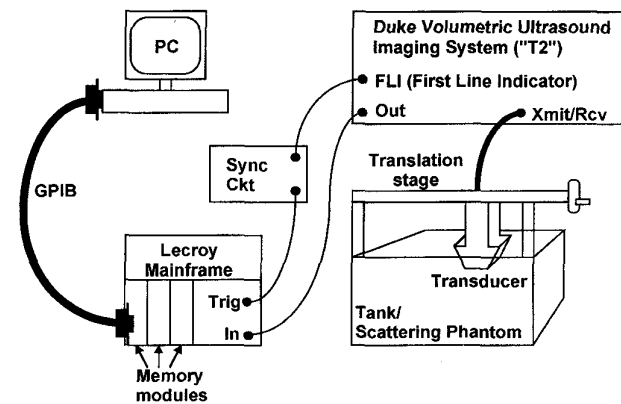


Fig. 2. Experimental setup.

used to acquire volumes of pulse-echo information from a scattering phantom. For each volume, a pyramid was scanned in which both the elevation and lateral sweep of the beam encompassed about  $16^\circ$ . The volumes were sampled using either  $0.5^\circ$  spacing ( $1024$  transmitted pulses,  $32 \times 32$  lines in the elevation-lateral dimensions) or  $0.25^\circ$  spacing ( $4096$  lines,  $64 \times 64$ ). The data acquired were range gated from  $82.5$  to  $102.5$   $\mu\text{s}$ , or from about  $62.5$  to  $77.0$  mm. The transmit focus was set at  $70$  mm, while the received field was dynamically focused every  $5$  mm.

The transducer used was a  $16.4$ -mm diameter circular transducer with a center frequency of  $2.4$  MHz, built at Duke University. The transducer was diced into a grid with an interelement spacing of  $0.4$  mm. The  $192$  transmit elements are arranged randomly with a Gaussian spatial distribution, and the  $64$  receive elements have a spatially even random distribution similar to that described by Davidsen *et al.* [14]. The transducer is fixed to a translation stage by a clamp that keeps its position constant relative to the mounting.

The blood phantom used was a container of densely packed gelatin-encapsulated graphite spheres (RMI, Inc.) in an alcohol bath (8% isopropyl alcohol solution) similar to that described by Madsen *et al.* [15]. The alcohol bath rises above the agar spheres such that the transducer may be displaced laterally while immersed in the fluid without disrupting the positions of the spheres themselves. A LeCroy digitizing recorder (LeCroy 8828D Waveform Digitizer) was used to sample the RF signals at  $50$  MHz, and the resulting data were transferred to a PC for off-line processing.

Two types of experiments were performed, one with lateral translation and the other with axial translation. Data for  $16$  volumes were taken in each of the two experiments. The transducer was moved relative to the blood phantom between volume acquisitions, thus simulating target motion. The phantom was moved in increments of  $1/50$  of an inch ( $0.508$  mm) for the lateral-translation experiment, and in increments of  $0.5$  mm for the axial-translation experiment.

### B. Off-Line Processing

The RF pulse-echo data from the scanned volumes ("volume data") were processed off-line to find 3-D peaks. The

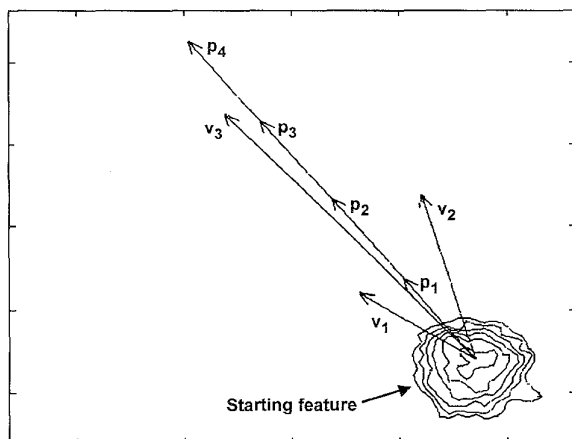


Fig. 3. Diagram of tracking process. The  $p$ 's represent actual translations while the  $v$ 's represent estimates.

data were first envelope detected using a Hilbert transform operation [16]. A gradient-type search was performed on the detected data in three dimensions, with points found to be local maxima recorded as features. With a list of the extracted feature coordinates from the first volume, peaks suitable for tracking were selected. Among the top 50 peaks in amplitude, those whose coordinates remained within the scanned volumes throughout the experiment were deemed suitable for tracking.

Starting with the second volume and continuing with successive volumes, an "expected position" was calculated for each feature due to the known translation. An expected position matrix,  $P$ , was formed, with elements  $p$  representing the  $x$ ,  $y$ , and  $z$  coordinates of the expected position for a certain feature. There are  $N$  elements in this matrix, with  $N$  being the total number of volumes interrogated

$$P = [\bar{p}_1, \bar{p}_2, \dots, \bar{p}_N]. \quad (1)$$

For every  $1 \leq k < N$ , then  $p_{k+1} - p_k$  is a 3-D vector representing the translation between volume interrogations. A search for the local maximum was performed, starting from the expected position  $p_k$ . The local maximum closest to this point was taken as a vector estimate of translation  $v_k$ . Thus another matrix,  $V$ , was formed, with elements  $v$  representing the coordinates of the estimated translation

$$V = [\bar{v}_1, \bar{v}_2, \dots, \bar{v}_N]. \quad (2)$$

An illustration of this process is shown in Fig. 3. For each experiment, the number of estimated translation vectors  $V$  formed corresponds to the number of features tracked. Each vector  $V$  is treated as an observation of the tracking process.

### III. RESULTS

A graph of the estimated translation versus real translation for the lateral and axial experiments is shown in Fig. 4. The mean of the estimated translations  $\hat{E}\{V[n]\}$  is the abscissa of each graph. The error bars represent  $\pm 1$  standard deviation of the magnitude of the translation estimates,  $\text{stdev}(\|V[n]\|)$ . The abscissa is labeled velocity ( $v$ ) times time ( $T$ ), or  $vT$  in mm, thus representing a range of velocities which depend on

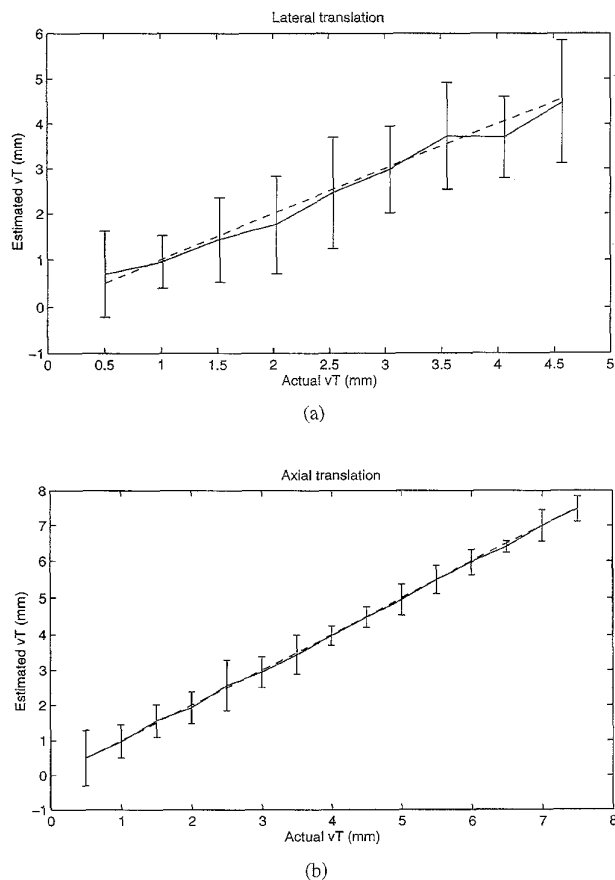


Fig. 4. Actual versus estimated translation for (a) lateral- and (b) axial-translation experiments.

the pulse repetition time ( $T$ ), which is  $1/\text{PRF}$  (pulse-repetition frequency). For example,  $vT = 0.5$  mm could represent a velocity of 0.5 m/s with a PRF of 1 KHz, or a velocity of 0.25 m/s with a PRF of 500 Hz.

The amplitude loss of the maxima in dB as a function of translation is shown in Figs. 5 and 6 for the lateral- and axial-translation experiments, respectively. This loss in amplitude is with respect to the amplitude of the starting peak (in the first volume), or

$$\text{loss}_{\text{dB}}[n] = \hat{E} \left\{ 20 \log \frac{A(\bar{v}[n])}{A(\bar{v}[0])} \right\} \quad (3)$$

where  $v[0]$  is the starting coordinate and  $A(v[n])$  is the signal amplitude at the coordinate represented by  $v[n]$ . As can be seen, the amplitude of the peak decreases slowly even with large translations. For comparison, the amplitude loss at the expected position ( $p$ ) is also shown. This graph drops more rapidly than the previous one since the actual peak was usually seen to deviate from the expected location, i.e., the expected position is usually slightly off the local maximum. The axial-translation loss is not as steep as the lateral-translation loss since the expected position in the axial dimension is closer to the true peak than in the lateral dimension, as discussed below.

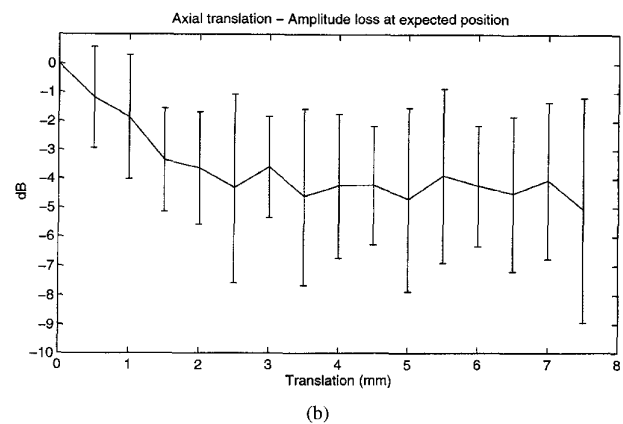
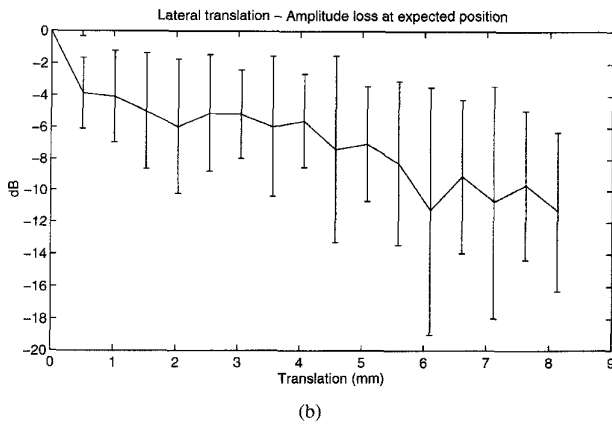
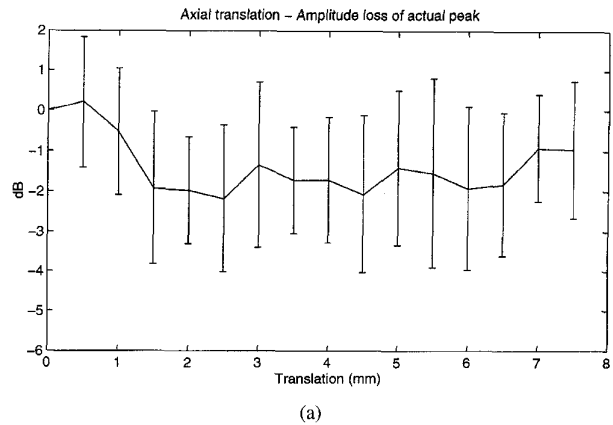
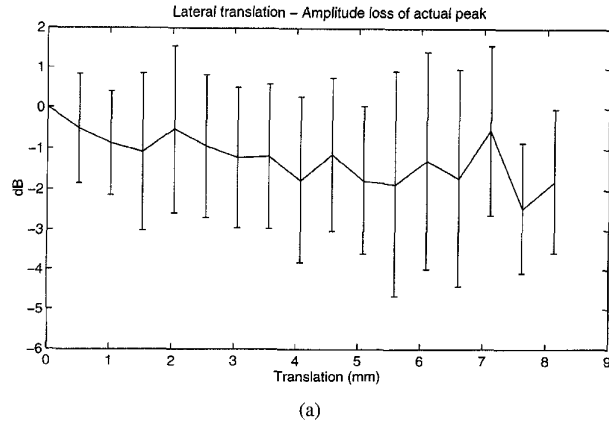


Fig. 5. Amplitude loss (a) of actual peak and (b) at the expected position for the lateral-translation experiment.

Fig. 6. Amplitude loss (a) of actual peak and (b) at the expected position for the axial-translation experiment.

Fig. 7 shows the distance from the expected position to the actual peak location for lateral and axial displacements. This can be denoted

$$w[n] = \hat{E}\{|\bar{\mathbf{v}}[n] - \bar{\mathbf{p}}[n]|\} \quad (4)$$

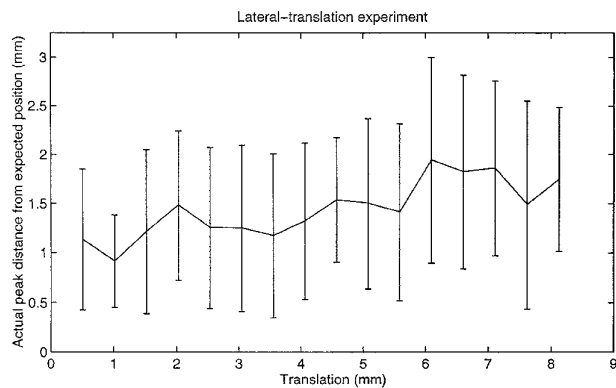
where  $w$  is the distance between  $\mathbf{v}$  and  $\mathbf{p}$  coordinates. It is seen that this distance slowly increases from about 1 to about 1.5–2 mm, with large error bars. It is interesting to decompose the vector  $\mathbf{v}-\mathbf{p}$  into its lateral and axial components; this is shown in Figs. 8 and 9 for lateral and axial displacements, respectively. The directional component of  $\mathbf{v}-\mathbf{p}$  in the lateral direction is much larger than that of the axial component in both the lateral-translation and axial-translation experiments.

#### IV. DISCUSSION

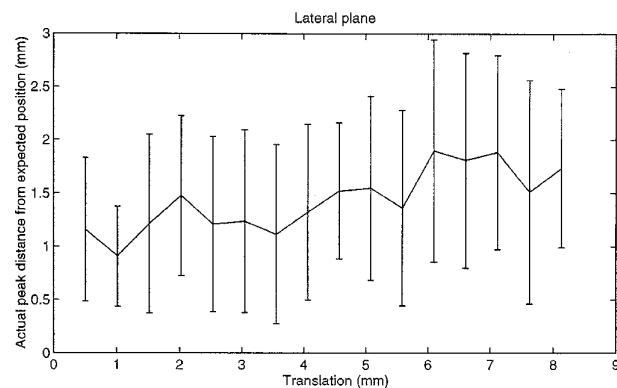
The feature tracking experiments show that local maxima in the received field can be used as markers to determine target motion. This tracking, however, is subject to limitations, as discovered during the experiments. The first limitation is the duration of the peak; that is, how far can the scatterers move before the local maxima no longer exists around the expected point? From Figs. 5 and 6 it can be seen that, in general, the peak amplitude slowly decreases with translation. At this point it was instructive to watch a “movie” in which frames were

constructed by slicing the data volume at a constant depth, i.e., a C-scan. As an example, three frames of one of these movies are shown in Fig. 10. The first frame shows a C-scan from the first volume, at a depth that corresponds to slicing through the middle of a 3-D local maxima. The  $X$  denotes the starting position, i.e., the local maximum in the first volume. The next frame shows a C-scan at the same depth, but a later volume, where the lateral translation is approximately 25% of the aperture diameter. The dotted line shows the expected movement of the peak, with the  $X$  representing the expected position in this volume and the  $O$  representing the estimated translation. The last frame shows the C-scan at a translation of 50% of the aperture diameter. At this point, the nearest peak to the expected position (denoted  $O$ ) is no longer the same peak as that from the first volume.

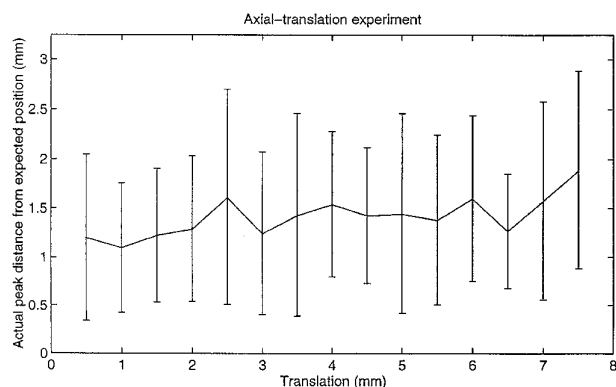
This limitation is particularly detrimental in the lateral-translation case. From watching many movies, it was seen that the peaks may be “safely” tracked at least to a distance of 0.25 of the aperture diameter. Between 1/4 and 1/3 of the aperture diameter, the amplitude decreases toward the overall mean of the speckle signal, making it harder to distinguish as a maximum. By the time the scatterers have translated 1/2 of the aperture diameter, the local maximum no longer exists. In the axial translation case, however, the peak may be safely tracked through a much greater distance.



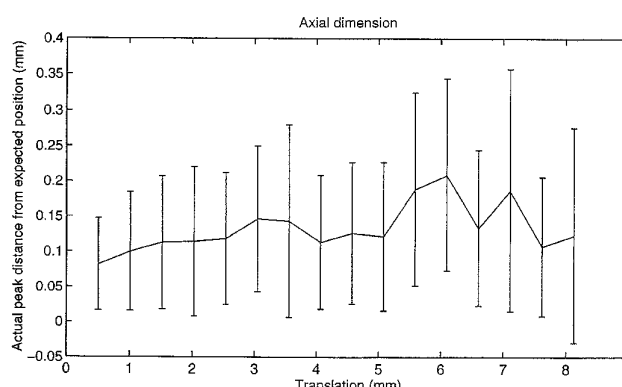
(a)



(a)



(b)



(b)

Fig. 7. Distance to actual peak from the expected position for the (a) lateral-translation and (b) axial-translation experiments.

Fig. 8. Distance to actual peak from the expected position: (a) projection onto lateral plane and (b) projection in the axial dimension for the lateral-translation experiments. Note the difference in the vertical scales between the top and bottom graphs.

Axial “misregistrations” (where the nearest-neighbor peak to the expected location is not the original peak) were less likely to occur throughout the experiment (an overall translation of about 7.5 mm) due to relatively slower speckle decorrelation in the axial dimension. In the axial-tracking movies, the peak was correctly tracked throughout the translation, unless the peak translated outside of the field of view. An example of three frames from an axial-translation experiment are shown in Fig. 11, where the first frame is the starting position, and the second and third frames denote translation distances of 3.5 and 7.0 mm, respectively.

The second limitation is the variation of the location of the peak around its expected position, i.e., the distance from the expected position to the actual location. Fig. 12 shows the distributions of the position of the true peak around the expected value in the  $x$ ,  $y$ , and  $z$  dimensions from the lateral-translation experiment. The distributions from the axial-translation experiment are similar and are not shown here. These distributions appear normal (skewness coefficients  $\alpha_{3,x} = 0.3$ ,  $\alpha_{3,y} = -0.2$ , and  $\alpha_{3,z} = 0.1$ ; kurtosis coefficients  $\alpha_{4,x} = 3.7$ ,  $\alpha_{4,y} = 3.2$ , and  $\alpha_{4,z} = 4.1$ ; for zero-mean Gaussian distributions  $\alpha_3 = 0$  and  $\alpha_4 = 3$ ), with standard deviations  $\sigma_x = 1.19$ ,  $\sigma_y = 1.10$ , and  $\sigma_z = 0.16$  mm. Since the statistics are not expected to be different between the elevation and lateral dimension, the  $x$  and  $y$  data may also

be combined as “lateral” observations. In this case,  $\alpha_{3,lat} = 0.1$ ,  $\alpha_{4,lat} = 3.4$ , and  $\sigma_{lat} = 1.15$ . As seen in Fig. 8, most of this uncertainty is in the lateral rather than the axial ( $z$ ) dimension. This limitation affects the magnitude of the error that can be expected for a certain translation. If the translation is about the same size as the uncertainty in locating the peak, errors on the order of 100% can be expected, while further translation will decrease the error. This refers to the absolute value of the error; however, the estimated translation of many observations will still average to the expected position, as shown in Fig. 4.

We have attempted to analyze the effect of the peak dither. If the density function of the actual feature location around the true translation is denoted  $f_v(R)$ , then the expected value of the magnitude velocity error will be

$$E\{|K|\} = \int_R \left| \frac{\|\mathbf{v}\| - \|\mathbf{p}\|}{\|\mathbf{p}\|} \right| f_v(R) dR \quad (5)$$

where  $\mathbf{v}$  is the estimated translation,  $\mathbf{p}$  is the true translation,  $K$  is the error, and  $R(x, y, z)$  is the region on which may be the actual feature location. If the magnitude of the true translation  $\mathbf{p}$  is a constant (as in our experiments), and if the regions over which  $\|\mathbf{v}\| > \|\mathbf{p}\|$  and  $\|\mathbf{p}\| > \|\mathbf{v}\|$  are known, then this integral

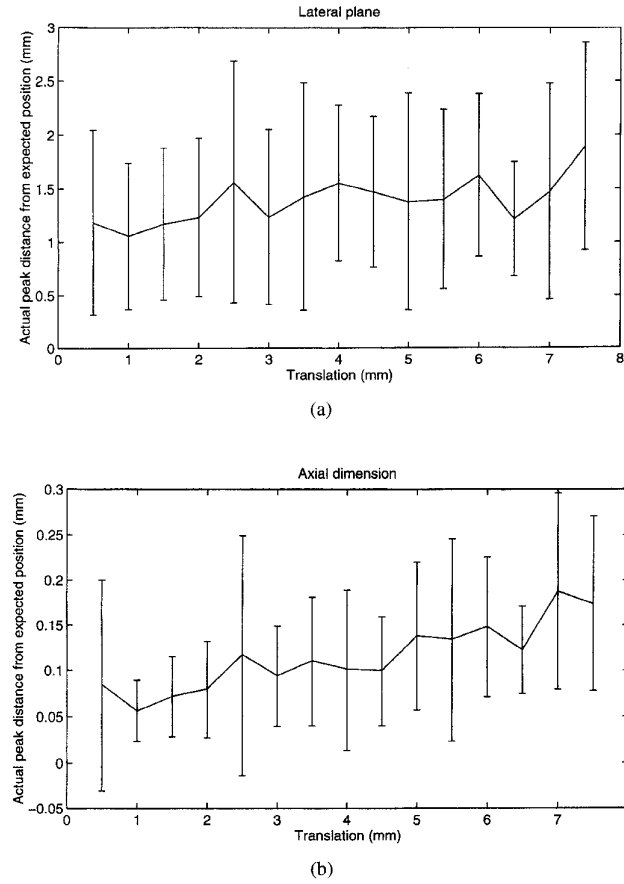


Fig. 9. Distance to actual peak from the expected position: (a) projection onto lateral plane and (b) projection in the axial dimension for the axial-translation experiments. Note the difference in the vertical scales between the top and bottom graphs.

may be evaluated by

$$E\{|K|\} = \frac{1}{\|\bar{\mathbf{p}}\|} \left( \int_{\|\bar{\mathbf{v}}\| > \|\bar{\mathbf{p}}\|}^R (\|\bar{\mathbf{v}}\| - \|\bar{\mathbf{p}}\|) f_v(R) dR + \int_{\|\bar{\mathbf{p}}\| > \|\bar{\mathbf{v}}\|}^R (\|\bar{\mathbf{p}}\| - \|\bar{\mathbf{v}}\|) f_v(R) dR \right). \quad (6)$$

Consider a 1-D case (see Fig. 13) with true translation  $\|\bar{\mathbf{p}}\| = d$  and a normally distributed true peak location around the true translation  $f_v(x)$

$$f_v(x) = \frac{1}{\sigma\sqrt{2\pi}} e^{-x^2/e^2\sigma^2}. \quad (7)$$

In this case,  $\|\bar{\mathbf{v}}\| = |x + d|$ . Equation (5) becomes

$$\langle |K| \rangle = \frac{1}{d\sigma\sqrt{2\pi}} \int_{-\infty}^{\infty} (|x + d| - d) e^{-x^2/e^2\sigma^2} dx. \quad (8)$$

Evaluating this integral gives

$$\langle |K| \rangle = \frac{\sigma}{d} \sqrt{\frac{2}{\pi}} \left( 1 - e^{-d^2/2\sigma^2} + e^{-d^2/2\sigma^2} \right) + 2 \operatorname{erf}\left(\frac{d\sqrt{2}}{\sigma}\right) - \operatorname{erf}\left(\frac{d}{\sigma\sqrt{2}}\right) - 1 \quad (9)$$

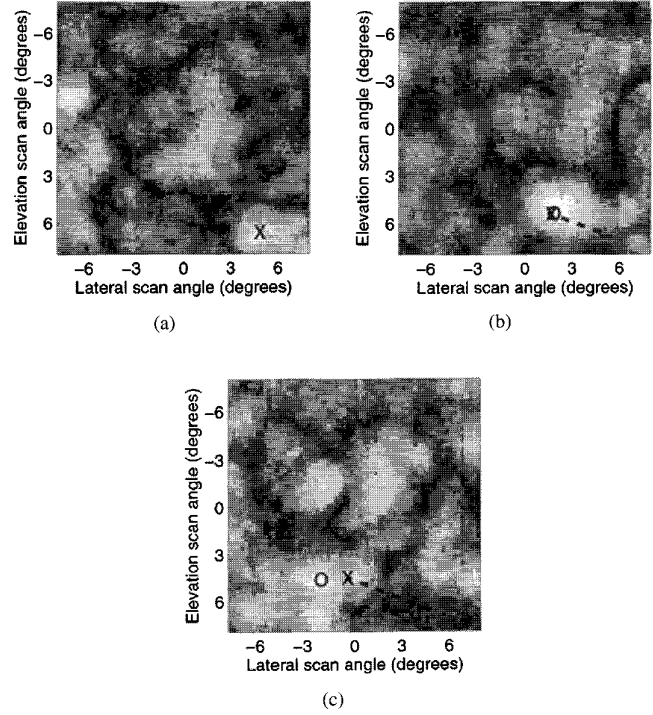


Fig. 10. Lateral translation movie frames: (a) starting position ( $X$  denotes the peak to be tracked); (b) after translation of  $1/4$  aperture diameter; and (c) after translation of  $1/2$  aperture diameter. In frames (b) and (c),  $X$  denotes the expected position, the dotted line denotes the expected path, and  $O$  denotes actual peak location.

where

$$\operatorname{erf}(x) = \frac{2}{\sqrt{\pi}} \int_0^x e^{-\xi^2} d\xi. \quad (10)$$

By the Cramér-Rao lower bound [17], a most-efficient estimate of the mean  $\hat{m}$  from  $N$  observations of a normally distributed random process  $f_n(m; \sigma^2)$  will itself be normally distributed with variance  $\sigma^2/N$ . That is

$$\operatorname{var}[\hat{m}] = \frac{\sigma^2}{N}. \quad (11)$$

Therefore if our estimate of translation  $v$  comes from  $N$  observations, the expected value of the absolute error in magnitude will be

$$\langle |K| \rangle = \frac{\sigma}{d} \sqrt{\frac{2}{\pi N}} \left( 1 - e^{-Nd^2/2\sigma^2} + e^{-2Nd^2/2\sigma^2} \right) + 2 \operatorname{erf}\left(\frac{d\sqrt{2N}}{\sigma}\right) - \operatorname{erf}\left(\frac{d}{\sigma} \sqrt{\frac{N}{2}}\right) - 1. \quad (12)$$

We can define a dimensionless parameter  $\zeta$

$$\zeta \equiv \frac{d\sqrt{N}}{\sigma} \quad (13)$$

so that (12) becomes

$$\langle |K| \rangle = \frac{1}{\zeta} \sqrt{\frac{2}{\pi}} \left( 1 - e^{-\zeta^2/2} + e^{-2\zeta^2} \right) + 2 \operatorname{erf}(\zeta\sqrt{2}) - \operatorname{erf}\left(\frac{\zeta}{\sqrt{2}}\right) - 1. \quad (14)$$

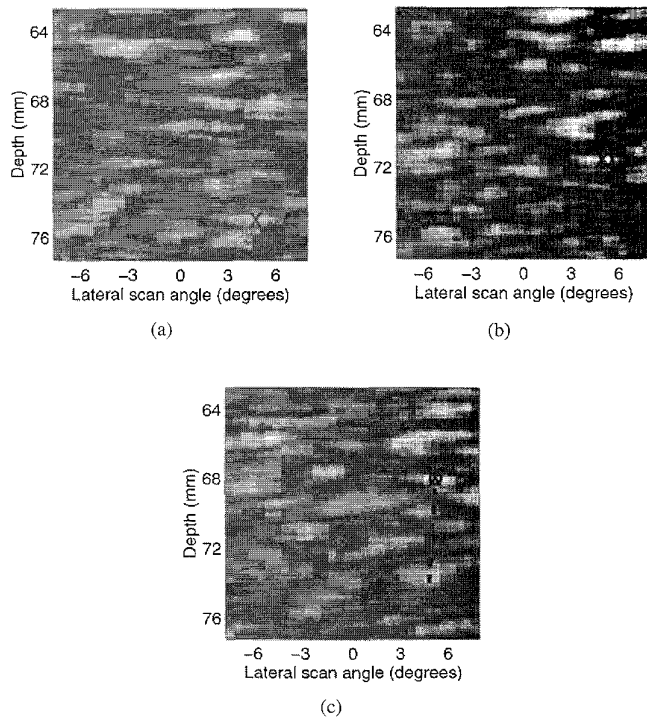


Fig. 11. Axial translation movie frames: (a) starting position ( $X$  denotes peak to be tracked); (b) after translation of 3.5 mm; and (c) after translation of 7.0 mm. In frames (b) and (c),  $X$  denotes the expected position, the dotted line denotes the expected path, and  $O$  denotes actual peak location.

TABLE I  
REQUIRED NUMBER OF OBSERVATIONS TO ACHIEVE A CERTAIN  
EXPECTED ABSOLUTE ERROR FOR CHOSEN VALUES OF  $d/\sigma$

$d/\sigma$	Maximum absolute %error desired	# Observations needed
3	20	2
2	20	4
1	20	16
1	40	4
0.5	40	16
0.5	20	64

A graph of this function is shown in Fig. 14. It is seen that  $|K|$  is inversely related to  $\zeta$ , which in turn is related to the translation distance, number of observations, and standard deviation of the original uncertainty distribution. For example, for a translation of 1 mm estimated from a distribution with 1 mm standard deviation, approximately 16 observations are needed to achieve an expected absolute error of 20%, while for the same translation and a distribution with 0.5 mm standard deviation, approximately four observations would be needed (the graph crosses the 20% line at approximately  $\zeta = 4$ ). Table I shows the number of observations needed to achieve a certain error percent for chosen translation distances and distribution standard deviations.

Since  $d = vT$  in our experiments, the inverse relationship between expected error and  $z$  may be rewritten

$$\frac{vT\sqrt{N}}{\sigma} \propto \frac{1}{|K|}; \quad \text{for } Q \geq \frac{1}{\sigma} \frac{\text{samples}}{\text{unit distance}}. \quad (15)$$

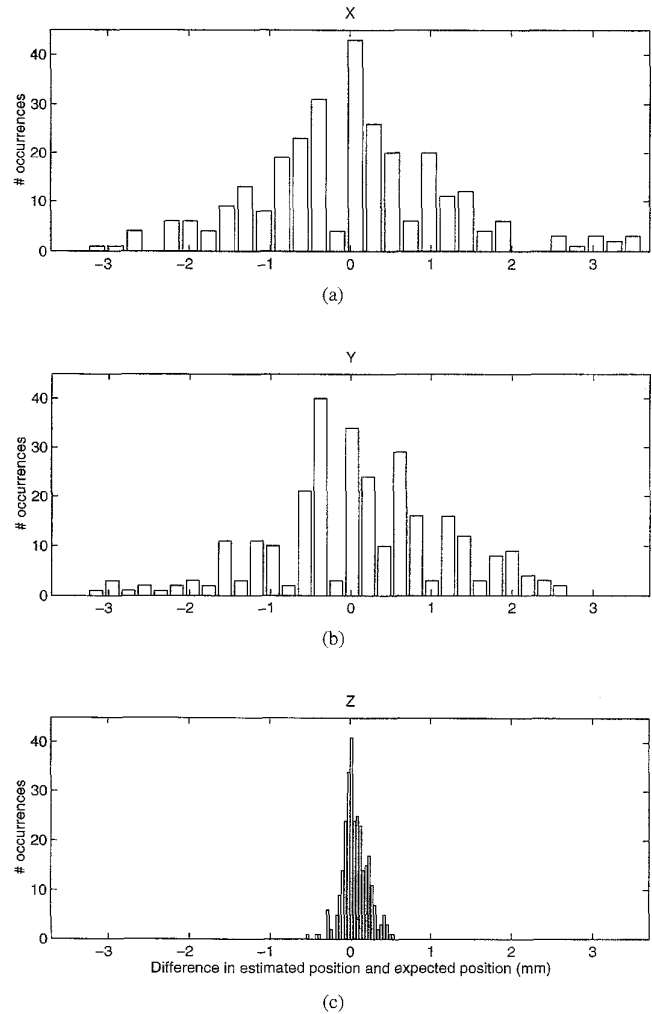


Fig. 12. Histograms of the position of the actual peak location around the expected location in the (a)  $x$ -dimension, (b)  $y$ -dimension, and (c)  $z$ -dimension.

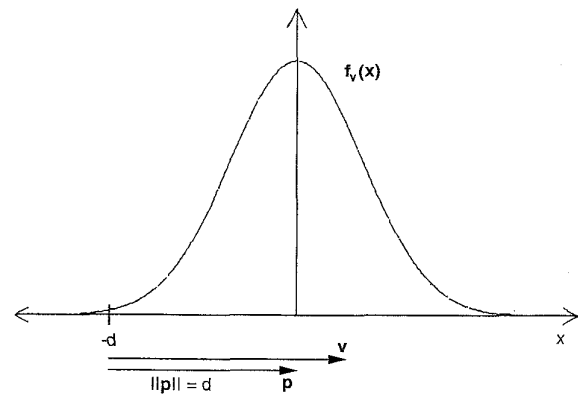


Fig. 13. One-dimensional case of velocity estimation. Vector  $p$  is the true translation from  $-d$  to the origin ( $\|p\| = d$ ). Vector  $v$  is the estimated translation, and  $f_v(x)$  is the density function of  $\|v\| - \|p\|$ .

Here,  $v$  is the magnitude of the velocity,  $T$  is the pulse repetition period,  $N$  is the number of interrogations (obser-



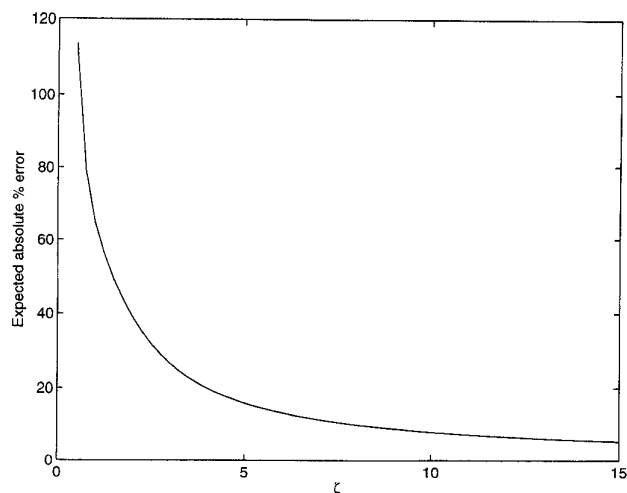


Fig. 14. Theoretical graph of expected absolute error versus  $\zeta$ .

variations), and  $K$  is the error, where we have added  $Q$  as the spatial sampling (samples/unit distance) to show adequate representation of the signal. If  $Q$  is much less than  $1/\sigma$ , higher errors due to undersampling will be present. Thus, increasing  $v$ ,  $T$ , or  $N$ , or decreasing  $\sigma$  will cause a decrease in the magnitude of the error. This inverse relation is verified in the experimental absolute error graphs shown in Fig. 15 for lateral and axial translations. Both curves show that as  $vT$  increases, the error decreases. This agrees with our theoretical prediction of inverse relationship (Fig. 14). Also, the error for the graph of the axial experiment is generally lower than that of the lateral-translation experiment, except after one observation. This is due to the probability that the peak is located closer to the expected value in the axial dimension than that of the lateral dimension, i.e.,  $\sigma_{\text{axial}} < \sigma_{\text{lateral}}$ . It should be noted that this theoretical development is valid for tracking one peak; tracking multiple peaks that are known to be moving at the same velocity will further reduce the expected error.

This relation holds true subject to the limitations described above, however. Once the sampling along a certain dimension is more than that of the uncertainty in that direction, increased sampling will not decrease the variance of the error. This was seen in two separate lateral-translation experiments in which the lateral sampling in one set of volumes was twice as fine as that of another set of volumes. All other parameters were the same between experiments. The error graphs and uncertainty graphs, not shown here, were essentially unchanged between the two sets of results.

Also, peaks cannot be tracked beyond the point where they disappear. In the lateral set of experiments, this turned out to be about  $1/4$  to  $1/3$  of the aperture diameter. In the axial set of experiments, this did not appear to be a problem for normal blood velocities in humans. This becomes important in a real-time algorithm for tracking peaks; the algorithm must be able to correspond maxima from one frame to the next and account for their genesis and fading away.

Finally, it is acknowledged that this simulation of moving tissue or blood by translation of a transducer over a scattering

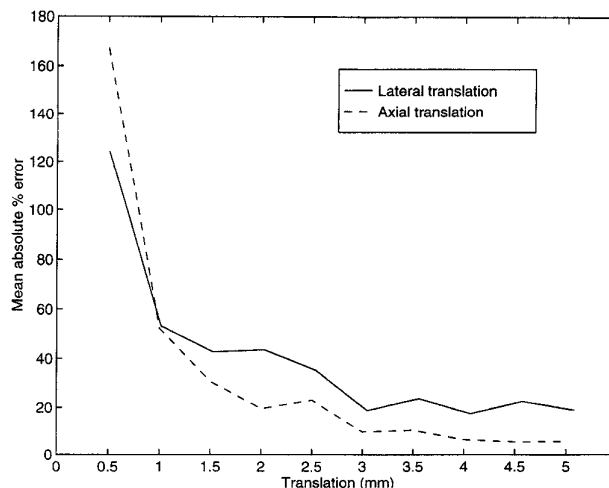


Fig. 15. Experimental mean absolute error versus translation for the lateral- and axial-translation experiments.

phantom represents an ideal situation, where the individual scattering particles remained fixed in location with respect to each other. In addition, the scatterers remained stationary over the time required to acquire a volume of pulse-echo information. Neither case would be true in *in vivo* tissue motion, especially in flowing blood where the scatterers (red blood cells) may be constantly rearranged. Our results are thus for a best-case scenario. It remains to be seen how these conditions, including profiled flow, rotational motion, redistribution of scatterers, etc., would affect the feature tracking process, especially the waxing and waning of peaks.

## V. CONCLUSIONS

We have shown that tracking a local maximum of ultrasound speckle in three dimensions is a valid approach to measuring target motion. Using a few observations, an estimation of the vector velocity can be made with reasonable accuracy. This approach is limited by the uncertainty in the location of the peak around the expected value, particularly in the lateral dimension; and the duration time of a local maximum. Since the location of a peak is more certain in the axial dimension, the expected error in that direction is less using this method. The application of this technique to blood flow instrumentation would permit accurate angle-independent blood velocity determination in three dimensions using potentially fewer observations than are required by current systems. The improvement in speed and lack of angle dependence have important implications for improving clinical diagnosis with flow imaging systems and quantifying tissue motion in the normal or abnormal myocardium.

## REFERENCES

- [1] C. B. Burckhardt, "Speckle in ultrasound B-mode scans," *IEEE Trans. Sonics Ultrason.*, vol. SU-25, pp. 1-6, 1978.
- [2] A. Kozma and C. R. Christenson, "Effects of speckle on resolution," *J. Opt. Soc. Amer.*, vol. 66, no. 11, pp. 1257-1260, 1976.
- [3] D. W. Baker, "Pulsed ultrasonic Doppler blood-flow sensing," *IEEE Trans. Sonics Ultrason.*, vol. SU-17, no. 3, pp. 170-185, 1970.

- [4] M. D. Fox, "Multiple crossed-beam ultrasound Doppler velocimetry," *IEEE Trans. Sonics Ultrason.*, vol. SU-25, pp. 281-286, 1978.
- [5] J. R. Overbeck, K. W. Beach, and D. E. Strandness, Jr., "Vector Doppler: Accurate measurement of blood velocity in two dimensions," *Ultrasound Med. Biol.*, vol. 18, no. 1, pp. 19-31, 1992.
- [6] P. J. Phillips, A. P. Kadi, and O. T. von Ramm, "Feasibility study for a two-dimensional diagnostic ultrasound velocity mapping system," *Ultrasound Med. Biol.*, vol. 21, no. 2, pp. 217-229, 1995.
- [7] G. E. Trahey, J. W. Allison, and O. T. von Ramm, "Angle independent ultrasonic detection of blood flow," *IEEE Trans. Biomed. Eng.*, vol. BME-34, pp. 965-967, 1987.
- [8] L. N. Bohs and G. E. Trahey, "A novel method for angle independent ultrasonic imaging of blood flow and tissue motion," *IEEE Trans. Biomed. Eng.*, vol. 38, pp. 280-286, 1991.
- [9] K. W. Ferrara, "Estimation of the beam-vessel angle and 3-D velocity magnitude," *IEEE Trans. Ultrason., Ferroelect., Freq. Contr.*, vol. 42, no. 3, pp. 416-428, 1995.
- [10] V. L. Newhouse, D. Censor, T. Vontz, J. A. Cisneros, and B. B. Goldberg, "Ultrasound Doppler probing of flows transverse with respect to beam axis," *IEEE Trans. Biomed. Eng.*, vol. BME-34, pp. 779-789, 1987.
- [11] D. N. Roundhill, "Ultrasound time domain velocity measurement," Ph.D. dissertation, Duke Univ., NC, 1991.
- [12] G. R. Bashford and O. T. von Ramm, "Speckle structure in three dimensions," *J. Acoust. Soc. Amer.*, vol. 98, no. 1, pp. 35-42, 1995.
- [13] H. G. Pavy, S. W. Smith, and O. T. von Ramm, "An improved real-time volumetric ultrasonic imager," *Med. Imag. V: Image Phys., SPIE*, vol. 1443, pp. 54-61, 1991.
- [14] R. E. Davidsen, J. A. Jensen, and S. W. Smith, "Two-dimensional random arrays for real time volumetric imaging," *Ultrason. Imag.*, vol. 16, pp. 143-163, 1994.
- [15] E. L. Madsen, J. A. Zagzebski, M. F. Insana, T. M. Burke, and G. Frank, "Ultrasonically tissue-mimicking liver including the frequency dependence of backscatter," *Med. Phys.*, vol. 9, pp. 703-710, 1982.
- [16] J. W. Gibson, *Principles of Analog and Digital Communications*. New York: Macmillan, 1989, p. 115.
- [17] C. W. Therrien, *Discrete Random Signals and Statistical Signal Processing*. Englewood Cliffs, NJ: Prentice-Hall, 1992, p. 292.
- [18] J. Meunier, M. Bertrand, G. Mailloux, and R. Petitclerc, "Assessing local myocardial deformation from speckle tracking in echography," *SPIE Med. Imag. II*, vol. 914, pp. 20-29, 1988.



Society of America.

**Gregory R. Bashford** (S'96) was born in Fayetteville, AR, in 1968. He received the B.S. degree in electrical engineering from the University of Nebraska, Lincoln, in 1991 and the Ph.D. degree in biomedical engineering from Duke University, Durham, in 1995.

He currently is an Instructor with the Department of Biomedical Engineering, Duke University. His interests include medical imaging, communications, signal processing, and theology.

Dr. Bashford is a member of the Acoustical



**Olaf T. von Ramm** was born in Posen, Poland, on August 16, 1943. He received the B.A.Sc. and M.A.Sc. degrees in electrical engineering from the University of Toronto, Ontario, Canada, in 1968 and 1970, respectively, and the Ph.D. degree in biomedical engineering from Duke University, Durham, in 1973.

He joined the faculty of Duke University in 1974 and currently holds the appointments of Professor of Biomedical Engineering, Director of the National Science Foundation/Emerging Research Center for Emerging Cardiovascular Technologies, and Assistant Professor of Medicine. He has served a variety of administrative roles at Duke University including: Director of Undergraduate Studies, Director of Graduate Studies, and Department Representative to the University's Academic Council. He has been interested in optical data processing, acoustical holography, the application of ultrasonic techniques to diagnostic medicine, and is involved in the development of advanced-phased array ultrasound imaging systems.

Dr. von Ramm has been a member of the Medical Science Advisory Panel to NASA and served on the Diagnostic Radiology Study Section of the National Institutes of Health from 1982 to 1988. He is a fellow of the American Institute of Ultrasound in Medicine and the American Society of Echocardiography.